

Interference-free Epipole-centered Structured Light Pattern for Mirror-based Multi-view Active Stereo

Tomu Tahara Ryo Kawahara Shohei Nobuhara Takashi Matsuyama
Graduate School of Informatics, Kyoto University
Yoshidahommachi, Sakyo, Kyoto, Japan
{tahara,kawahara,nob,tm}@vision.kuee.kyoto-u.ac.jp

Abstract

This paper is aimed at proposing a new structured light pattern for mirror-based multi-view active stereo so that the patterns cast onto the object surface do not interfere even where the object is illuminated by the projector directly and indirectly via mirror. The key idea of our interference-free projection is to encode the projector pixel locations so that they do not collide with the code from other projector pixels by exploiting the epipolar geometry defined by the real and the virtual projectors. We prove that our new encoding does not generate code collisions between the direct and indirect patterns from the real and the virtual projectors respectively. Evaluations using real and synthesized datasets demonstrate that our approach can realize an interference-free projection without using specialized equipment such as orthographic projectors used in the state-of-the-art methods.

1. Introduction

Image-based full 3D capture of objects has been a fundamental challenge in computer vision for long years, and many studies have proposed various approaches depending on different scenarios such as dynamic performance capture [5, 8, 24, 25, 27], large-scale capture [1, 11, 13], non-Lambertian object capture [2, 10, 19], and so forth. In recent years, the rapid development of 3D printers led to an increasing demand for high-quality and affordable full 3D scanning systems.

The active stereo with structured lighting [18, 22, 28] is known as one of the practical solutions to achieve such goal, and this paper proposes a new structured light algorithm for a projector-camera pair equipped with mirrors. Our projector casts specially-designed structured light patterns onto the object surface, and our camera captures the object with coded textures from multiple virtual viewpoints defined by the mirrors.

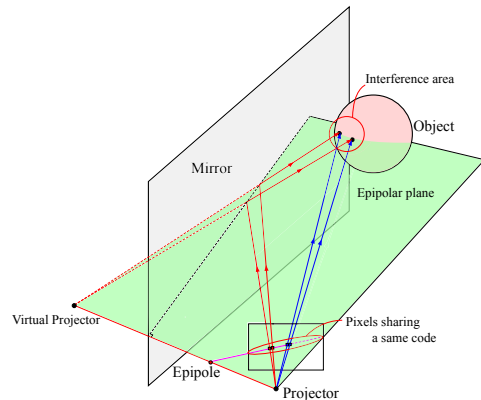


Figure 1. Epipole-centered structured lighting. Codes assigned according to the epipolar line do not produce interferences, since the rays emitted from pixels on an epipolar line can interfere only with rays passing through the same epipolar line.

The essential challenge in this paper is to handle interferences between the direct illumination from the projector and the indirect illumination via the mirror. Obviously casting traditional patterns such as the gray codes encoding the x , y locations of the pixels results in code collisions between the patterns cast directly and indirectly on the object surface.

The key idea on solving this interference problem is to encode the pixel locations using a polar coordinate system that is defined by the epipolar geometry between the real and the virtual projector (Figure 1). We prove that our patterns generated according to the epipolar lines do not result in code collisions theoretically, regardless of the object 3D shape and location.

Compared with the state-of-the-art [16] that also handles the interferences in a projector-camera system with mirrors, our contribution is twofold. Our method (1) works with regular perspective projectors, and (2) the projector is not necessarily arranged physically in a specific configuration against the mirrors. We believe these points make mirror-based full 3D capture methods more practical, in comparison with the state-of-the-art that requires an orthographic

projector physically aligned perpendicular to the intersection of the mirrors in order to suppress the collisions.

2. Related Work

In the field of computer vision, full 3D capture of the object has been studied in many contexts, such as structure-from-motion [6,20], depth fusion [13,17], multi-view stereo [5,8,24,25,27], model fitting [4,9], etc. These studies can be characterized mainly by two aspects, (1) how they obtain the depth, and (2) how they capture the target from different views.

A straightforward solution to obtain accurate 3D depths is to use ToF sensors. In [13], Ikeuchi *et al.* have proposed a method that fuses 3D depth maps captured by ToF sensors at different positions. Except such sensors, active methods utilizing controllable illuminations are known to be robust especially for texture-less objects. For example Hernandez *et al.* [12] and Vlasic *et al.* [26] have proposed photometric stereo systems for full 3D capture. Also the active stereo is used for real-time depth capture [21]. Among these studies, the structured light approach is known to be an affordable solution for static objects to obtain accurate depths by casting coded illuminations from a projector onto the object surface [18,22,28].

Obtaining depths from different viewpoints has been realized by spatial, temporal, or mirror-based multi-view strategies where the object is captured by distributed cameras [5,8,24–27], by a moving camera [6,12,20], or by virtual cameras defined by mirrors [7,14] respectively. The first approach is well suited for dynamic object capture, but requires having multiple cameras installed. The second approach requires only a single camera, but requires calibrating the moving camera poses on the fly. The last approach can be a good compromise on realizing an affordable and robust system since it does not require multi-view cameras nor dynamic camera calibration.

In order to leverage the advantages of the structured-light and the mirror-based multi-view capture, Lanman *et al.* have proposed a system based on an orthographic pattern projection [16]. They showed that the code collisions between the direct projection and the indirect projection via the mirror can be suppressed by projecting patterns so as to be orthogonal to the intersection of the mirrors. As a result, their method requires an orthographic projector whose optical axis is physically aligned to be perpendicular to the intersection of the mirrors.

Compared with this state-of-the-art, our method (1) can realize an interference-free structured lighting with a regular perspective projector, and (2) does not require physically arranging the projector in a specific configuration according to the mirrors.

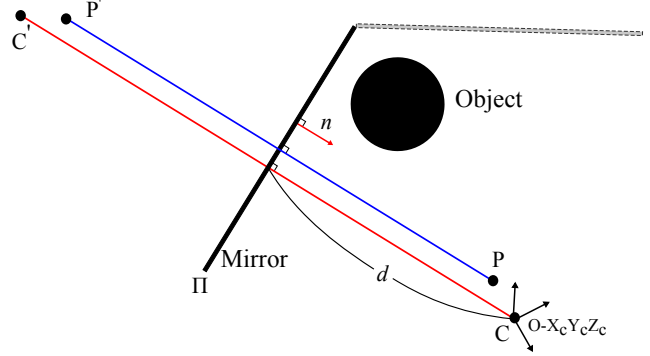


Figure 2. Measurement Model. The geometry by the other mirror (the dotted line above the object) is omitted for simplicity.

3. Measurement Model

As illustrated in Figure 2, we assume that the object is lit by a perspective projector P , and is captured by a perspective camera C . The mirror Π of distance d and normal \mathbf{n} is located behind the object so that the object is lit also by the virtual (or mirrored) projector P' , and also is captured by the virtual camera C' . Notice that although we use two mirrors for a full 3D capture as described later, this figure illustrates only one of them for simplicity. Also we use the camera coordinate system as the world coordinate system hereafter unless otherwise noted.

The camera and the projector are supposed to be calibrated beforehand using conventional methods [29] [15]. That is, a 3D point \mathbf{X} in the camera coordinate system is projected to

$$\lambda_c(u, v, 1)^\top = A_c \mathbf{X}, \quad (1)$$

in the camera image, and to

$$\lambda_p(u, v, 1)^\top = A_p(R_p \mathbf{X} + \mathbf{t}_p), \quad (2)$$

in the projector image. Here A_c and A_p denote the intrinsic parameters of the camera and the projector, R_p and \mathbf{t}_p denote the rotation and translation of the projector w.r.t. the camera respectively. λ_c and λ_p denote the depths from the camera and the projector respectively.

The distance d and the normal \mathbf{n} of the mirror Π are calibrated simply by capturing a chessboard by the camera C . By locating a chessboard so that C captures both the direct and mirror images of the chess corners, we can obtain the 3D positions of them in the camera coordinate system by applying Zhang method [29] separately for them. By denoting the 3D position of the i th corner by \mathbf{b}_i and its mirror by $\mathbf{b}'_i (i = 1, \dots, B)$, \mathbf{n} is given by

$$\mathbf{n} = \frac{\mathbf{n}'}{\|\mathbf{n}'\|}, \quad \mathbf{n}' = \frac{1}{B} \sum_{i=1}^B (\mathbf{b}_i - \mathbf{b}'_i), \quad (3)$$

and d is given by

$$d = -\frac{1}{B} \sum_{i=1}^B \mathbf{n}^\top \left(\frac{\mathbf{b}_i + \mathbf{b}'_i}{2} \right). \quad (4)$$

Notice that these parameters are further optimized non-linearly by a bundle adjustment process that minimizes the reprojection errors of 3D points triangulated from corresponding points in C, C', P, P' given by detecting identifiable feature points from camera images that are originally cast from the projector to the scene.

4. Interference-free Epipole-centered Structured Light Pattern

4.1. Design Policy

Obviously, code collisions can occur only where the object is multiply illuminated directly by the projector and indirectly via the mirror. In order to handle code collisions, one might consider a system in which the object is never illuminated multiply. However, designing such a mirror configuration and projector patterns is not possible without knowing the object 3D shape a priori. Hence similarly to the state-of-the-art [16], our system allows the object to be multiply illuminated, and we assume that we cannot predict such areas as we do not know the 3D geometry of the object.

Suppose a binary pattern (each pixel casts either ‘0’ or ‘1’) is projected to the object. In each of multiply illuminated areas, the codes can be

Case 1 a same even they are cast from different projector pixels, *i.e.*, the code from P and P' is both ‘0’ or ‘1’, or

Case 2 different, *i.e.*, the codes from P and P' are ‘0’ and ‘1’ (or ‘1’ and ‘0’).

Case 1 does not produce a code collision, even though the object is illuminated by different projector pixels, *i.e.*, directly by one pixel and indirectly by another. On the other hand, Case 2 results in a collision.

The goal of this paper is to introduce a projector pattern that never results in Case 2 regardless of the object 3D shape and position, by exploiting the epipolar geometry defined by the real perspective projector P and its mirror P' .

4.2. Epipolar Geometry between Real and Virtual Projectors

Consider the epipolar geometry between the perspective projector P and its mirror P' as illustrated in Figure 3. The key idea on realizing an interference-free structured lighting is to utilize the following proposition.

Proposition 4.1. *If a 3D point X illuminated directly by a projector pixel p is also illuminated indirectly by another*

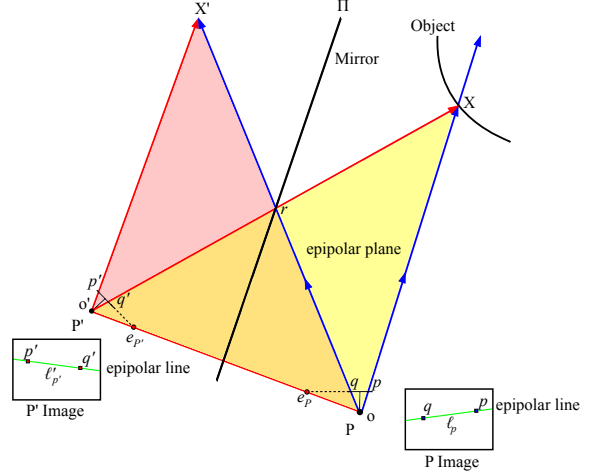


Figure 3. Epipolar geometry between the real projector P and the virtual projector P' .

projector pixel q via the mirror Π , q can exist only on the epipolar line ℓ_p passing through p and the epipole e_P in the projector image.

Proof. Consider illuminating a 3D point X behind a projector pixel p by another projector pixel q indirectly. By introducing X' , the mirror of X , as shown in Figure 3, this is equal to illuminating X' directly by the pixel p' of P' given as the mirror of p , and also directly by the projector pixel q .

The epipolar geometry between P and P' guarantees that q exists only on the epipolar line given as the intersection of the projector screen and the epipolar plane defined by the real projector center o , the virtual projector center o' , and the point p' in question. Here, since P and P' are symmetrically identical, p is also on the same plane, and hence the epipolar line passes through p as well.

From these results, we can conclude that the pixel q indirectly illuminating X can be only on the epipolar line ℓ_p passing through the epipole e_P and the pixel p illuminating X directly. \square

Proposition 4.1 suggests that as long as the projector pixels on an epipolar line ℓ_p share a same code, they never result in code collisions by definition since any 3D point illuminated by a pixel on ℓ_p can be illuminated indirectly only by another pixel on the same ℓ_p . Hence we can conclude that encoding the pixel locations based on the polar coordinate system centered at the epipole e_P provides an interference-free structured lighting for the perspective projector-camera system with mirrors.

Notice that this epipole-centered polar encoding is equivalent to rectifying the real and the virtual projector images utilizing the same epipole-centered polar coordinate system as proposed in [20]. This process decomposes the

image into a pencil of lines that is identical to the intersection of the projector screen and the sheaf of planes whose axis is the baseline direction. Since the baseline direction is equal to the normal \mathbf{n} of the mirror Π , each of the plane of the sheaf is always perpendicular to the mirror, and performs as a plane of reflection (Figure 1). Hence any pixels on such a plane, *i.e.*, on an epipolar line, can collide only with pixels on the same epipolar line.

Also, it should be noted that this proposition holds regardless of the object 3D geometry and the camera pose, since it depends only on the epipolar geometry between the projector P and its mirror P' defined by the mirror Π .

4.3. Interference-free Structured Light Pattern Generation

Proposition 4.1 guarantees that assigning a code on a per epipolar-line basis realizes an interference-free structured lighting. In practice, the pattern image is given by the following procedure.

- Step 1. Compute the epipole $e_P = (u_e, v_e)$ in the projector image frame.
- Step 2. Compute the angle θ of the polar coordinate (r, θ) for each point (u, v) in the projector image by $\theta = \tan^{-1}\left(\frac{v-v_e}{u-u_e}\right)$.
- Step 3. Encode θ by N -bits gray code as $g(u, v)$.
- Step 4. For each of N bits, generate a binary image from $g(u, v)$.

Figure 12 shows some examples of generated patterns.

5. Full 3D Capture by Structured Lighting with Multiple Mirrors

5.1. Triangulation

The pattern generated in Section 4.3 encodes the angle θ of the polar coordinates. In other words, decoding the code for each camera pixel x returns a corresponding epipolar line $\ell_p(x)$ emanating from the epipole e_P in the projector image defined by the epipolar geometry between the real projector P and the virtual projector P' as shown in Figure 4.

Similarly by considering the epipolar geometry between the camera C and the real projector P , the projector pixel y corresponding to the camera pixel x can appear only on the epipolar line $\ell_c(x)$ emanating from the epipole e_C in the projector image (Figure 5). As a result, y can be given as the intersection of $\ell_p(x)$ and $\ell_c(x)$.

Notice that y cannot be given uniquely if $\ell_p(x)$ and $\ell_c(x)$ are parallel. In particular, if the camera C and the projectors P and P' are collinearly located to each other, the two

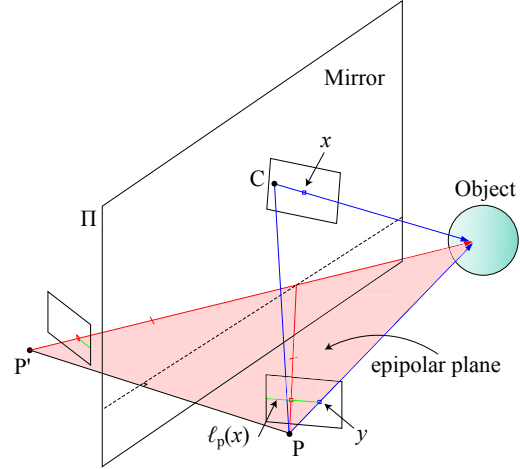


Figure 4. $P - P'$ epipolar geometry.

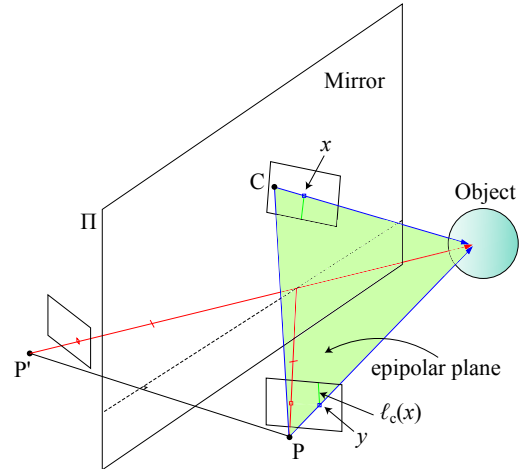


Figure 5. $P - C$ epipolar geometry.

epipoles e_P and e_C coincide and hence $\ell_p(x)$ and $\ell_c(x)$ become always identical to each other. These degeneracies can be detected easily in practice, because the positions of the two epipoles are given explicitly by the calibration.

Also it should be noted that triangulated 3D points appear behind the mirror if and only if their corresponding camera pixels observed the object via the mirror. Once detected such points, they should be reflected w.r.t. the mirror to obtain the real 3D geometry.

5.2. Structured Lighting with Multiple Mirrors

Up to this point we have considered the case of a single mirror system that can obtain the depths from the real and the virtual viewpoints. In order to realize a full 3D capture, our system should integrate additional views defined by different mirrors.

In this scenario, it should be noted that the structured light pattern in Section 4.3 can be valid only for a particular virtual view defined by a mirror. In case of multiple mirrors,

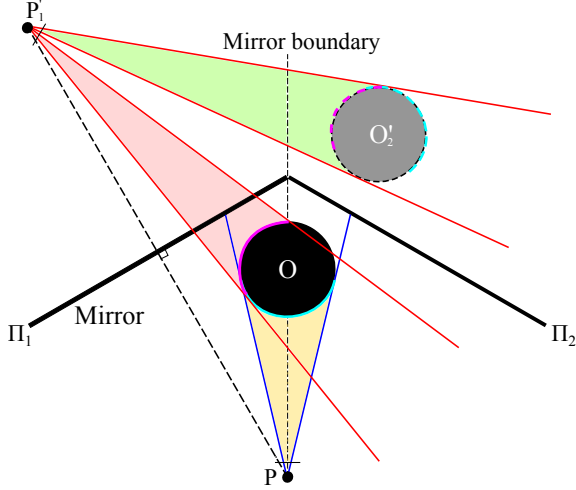


Figure 6. A mirror configuration without multiple reflections. If the virtual projector P'_1 by a mirror Π_1 does not observe the virtual object O'_2 defined by the other mirror Π_2 , the rays reflected twice or more cannot illuminate the object.

we can subdivide the projector image into disjoint regions so that pixels of each area illuminate a same mirror, and project the pattern on a per-region basis as shown in Figure 12.

Also the pattern in Section 4.3 is defined for the real projector and its mirror. That is, our method cannot handle multipath illuminations caused by multiple reflections between mirrors. This is a limitation of our approach, but it is possible to arrange the mirrors so as to have no multiple reflections in practice as shown in Figure 6.

5.3. Algorithm

Based on the above-mentioned considerations, we introduce the following algorithm as our interference-free epipole-centered structured light pattern for mirror-based full 3D capture of the object 3D shape.

- Step 1. Arrange the mirrors so that they do not have multiple reflections from the projector viewpoint (Section 5.2).
- Step 2. Calibrate the camera, the projector, and the mirrors parameters (Section 3).
- Step 3. Subdivide the projector image into regions corresponding to each of the mirrors based on the calibration (Section 5.2).
- Step 4. Generate structured light patterns for each mirror (Sections 4.3 and 5.2), as shown in Figure 12.
- Step 5. Capture images under the structured lighting, and decode θ at each camera pixel x to find the corresponding epipolar line $\ell_p(x)$ (Section 5.1).

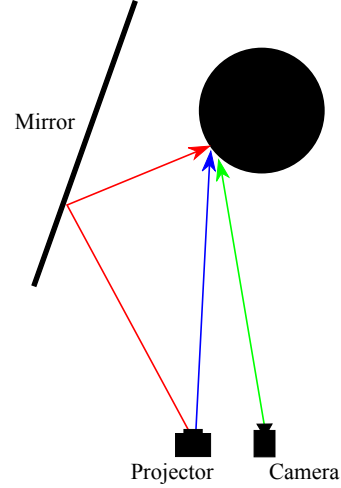


Figure 7. Simulation environment.

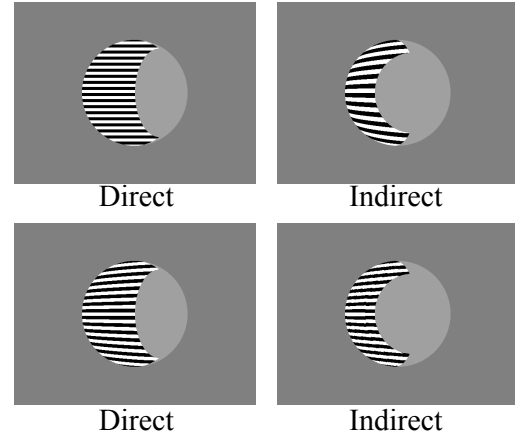


Figure 8. Example of images generated using direct and indirect illuminations. Top: conventional horizontal pattern. Bottom: proposed pattern.

- Step 6. For each projector image region, triangulate the 3D points and reflect the mirrored points (Section 5.1).
- Step 7. Merge the all 3D point clouds and return it as the 3D geometry of the object.

6. Evaluations

This section evaluates the performance of the proposed method quantitatively with a synthesized dataset and qualitatively with a real dataset.

6.1. Quantitative Evaluation with Synthesized Data

Figure 7 illustrates the simulation environment. The resolutions of the projector and the camera are set to 640×480 . The projector, the camera, and the mirror parameters (Sec-

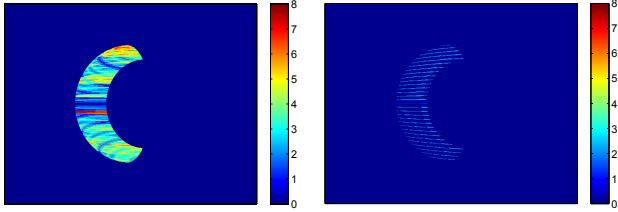


Figure 9. Distribution of the number of code collisions. Left: conventional horizontal pattern. Right: proposed pattern.

tion 3) are given as follows:

$$A_c = A_p = \begin{pmatrix} 320 & 0 & 320 \\ 0 & 320 & 240 \\ 0 & 0 & 1 \end{pmatrix}, \quad (5)$$

$$R_p = \begin{pmatrix} 1 & 0 & 0 \\ 0 & 1 & 0 \\ 0 & 0 & 1 \end{pmatrix}, \quad \mathbf{t}_p = \begin{pmatrix} 3 \\ 0 \\ 0 \end{pmatrix}, \quad (6)$$

$$\mathbf{n} = \begin{pmatrix} 0.9701 \\ 0 \\ -0.2425 \end{pmatrix}, \quad d = 5.0932, \quad (7)$$

and the target object is a sphere of radius $R = 2.0$ centered at $(0, 0, 5)^\top$. The images only by the direct illumination and only by the indirect illumination are synthesized separately by ray-tracing. Notice that the environment is assumed to have no ambient illumination, and each of the object point lit by a projector pixel of code “0” is assumed to appear as a “black” pixel in the camera image. Similarly each point lit by a projector pixel of code “1” appears as a “white” camera pixel for simplicity. The camera and the projector are assumed to have no lens distortions.

Figure 8 shows examples of synthesized camera image pair for a particular bit of our pattern and a conventional horizontal pattern. By comparing the colors pixel-by-pixel between these two direct and indirect images, code collisions can be detected as pixels having different colors (black and white).

Result Figure 9 shows pixel-wise counts of collided bits after projecting 9 patterns (9 bits) by the proposed method and the regular horizontal gray code encoding y values. In this figure, the blue color indicates pixels without code collisions, and the red color indicates pixels with collisions at 7 or more bits.

From this result, we can observe that our encoding successfully suppresses the code collisions compared with the regular pattern. Notice that we can still observe some collisions in our result (cyan lines in Figure 9 right). They correspond to code boundaries, and caused by quantization errors due to encoding along with slant epipolar lines.

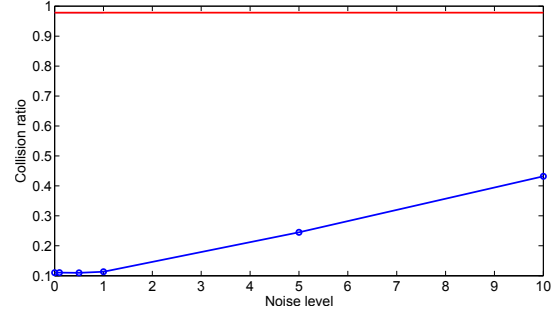


Figure 10. Ratios of code collisions at different noise levels. Red: conventional pattern. Blue: proposed pattern generated using epipoles with noise injected.

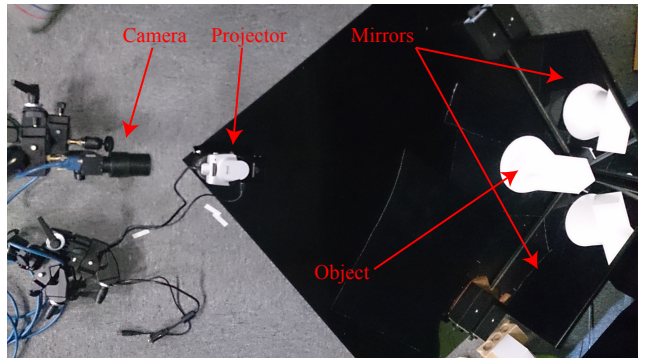


Figure 11. Experimental environment.

Figure 10 plots the ratio of pixels with collisions under different noise level in order to evaluate the robustness of the proposed encoding against calibration errors. In this evaluation, zero-mean Gaussian noise of $\sigma = 0.1, 0.5, 1, 5, 10$ px has been injected to the epipole position on generating our patterns, while the calibration parameters used for ray-tracing are unchanged. The blue plot indicates the average ratios of 1000 trials at each noise level. The red line illustrates the ratio of the regular horizontal pattern case without noise. By comparing these two plots, we can conclude that our pattern shows better performance even under noise of a few pixels.

6.2. Evaluation Real Images

Environment Figure 11 shows our experimental environment. A plaster object of approximately 20cm size is surrounded by two first surface mirrors behind it. We used a camera of 1280×960 resolution (Pointgrey Flea3 FL3-U3-13E4C) and a laser projector of 640×480 resolution (SHOWWX + Laser Pico Projector) in order to obtain focus-free projections that guarantee both the direct pattern and the indirect pattern via the mirror are in focus.

The calibration parameters were estimated by capturing chess patterns as described in Section 3. The average reprojection error after the bundle adjustment was 0.36 pixels.



Figure 12. Generated patterns for the left (top) and the right (bottom) mirrors.

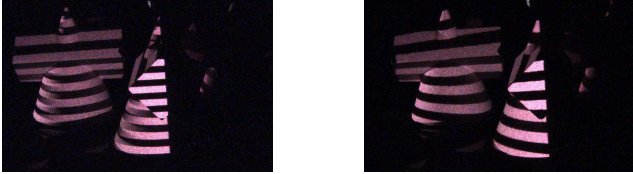


Figure 13. Example of captured images. Left: conventional horizontal pattern. Right: proposed pattern.

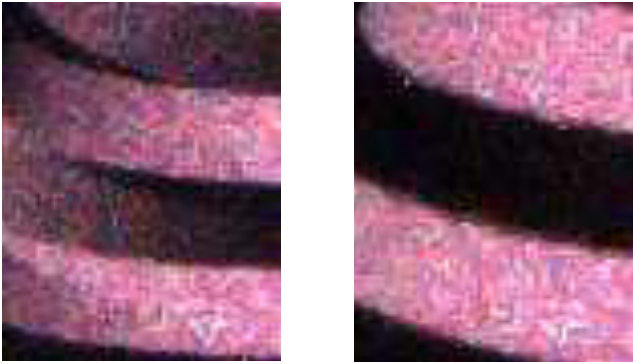


Figure 14. Close-up view of multiply illuminated areas in Figure 13. Left: conventional horizontal pattern. Right: proposed pattern.

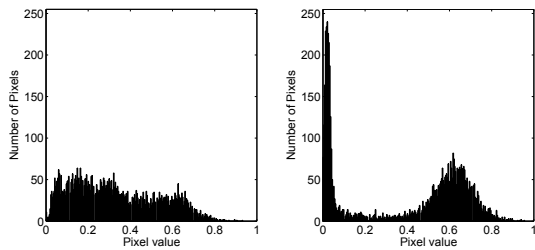


Figure 15. Normalized intensity histograms of Figure 14. Left: conventional horizontal pattern. Right: proposed pattern.

Result Figure 12 shows patterns generated based on the proposed method, and Figure 13 shows examples of captured images. Figure 14 shows a close-up view of an area with code collisions in Figure 13.

From these images, we can observe that the regular horizontal pattern results in code collisions where the object is multiply illuminated directly and indirectly, while our pattern successfully remove such interference. This fact can be

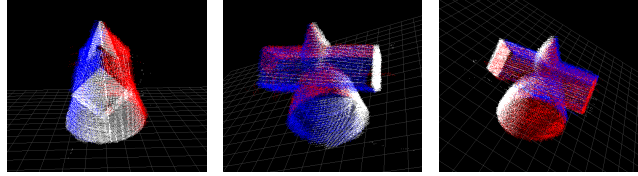


Figure 16. Reconstructed 3D shape rendered from different view-points. White, blue, and red points indicate 3D points triangulated using camera pixels in direct, left-mirror, and right-mirror views.

verified also by investigating the intensity histograms within the areas in question. Figure 15 shows the histograms normalized using the min/max values within the area. Compared with the histogram of the conventional horizontal pattern (Figure 15 left), the intensity distortion of our pattern (Figure 15 right) is clearly bimodal, that contributes achieving a robust decoding.

Figure 16 shows the 3D point cloud computed by triangulating the correspondences between the real camera and the two virtual projectors. The white, blue, and red dots indicate the points obtained from the real image, the mirrored points obtained from the virtual image by the left mirror, the mirrored points obtained from the virtual image by the right mirror respectively.

This result experimentally proves that our interference-free structured lighting concept can be achieved even under an imperfect calibration with practical reprojection errors.

6.3. Discussions

Generalization of Proposition 4.1 The proof of Proposition 4.1 described in Section 4.2 assumed a pair of real and virtual projectors. This proposition can be generalized for any projector pairs by assigning a code on a per epipolar plane basis.

That is, as illustrated in Figure 3, as long as the pixels of both projectors on a single epipolar plane share a same code, they illuminate object points on the plane with the same color.

Simultaneous pattern projection for different mirrors

Unfortunately our algorithm cannot produce a single pattern that provides an interference-free pattern projection for two or more mirrors simultaneously in general. This is because of the fact that our pattern utilizes the epipole-centered polar coordinate system. That is, if the pattern for the first mirror is identical to the one for the second mirror, the two epipoles on the projector image screen must coincide. This can be satisfied only if the mirrors are identical or parallel.

Alternatively, one may consider merging the patterns for different mirrors based on the apparent mirror regions in the projector image. This works without interferences if multiple illuminations via different mirrors do not occur. However, this configuration indicates that the object is not

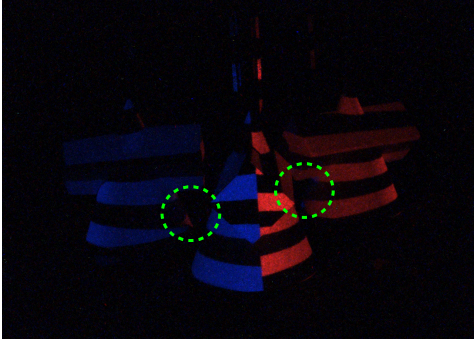


Figure 17. Captured image of a combined pattern for the mirrors. In the dotted circles, we can observe reflections overlapped with each other (red patterns in the left blue side, and blue patterns in the right red side).

fully covered by the structured illumination, and hence the system cannot capture the full 3D geometry. Hence as introduced earlier, our algorithm casts the patterns on a per-mirror basis.

One straightforward solution is to utilize the color-based multiplexing strategy [3]. That is, we can integrate the left and the right patterns (Figure 12) into a single image using different colors such as blue for the left and red for the right (Figure 17). By demultiplexing the image by the colors, we can obtain the images effectively identical to the ones captured with the per-mirror patterns.

Notice that this can handle only the interference between single reflections from different mirrors, and does not work if the system has multiple reflections (Figure 6).

Projector pattern aliasing Since our pattern utilizes a polar coordinate system, the code boundaries do not run horizontally nor vertically along the pixel directions. Besides, due to the radial structure of our pattern, each image region corresponding to a code can have different thickness according to the distance from the epipole. In particular, the pixels around the epipole can have sub-pixel thickness. This results in an aliased moiré pattern which makes establishing a pixel-by-pixel correspondences between the camera and the projector difficult.

Such aliasing issues can be suppressed by employing continuous-valued pattern, *e.g.* sinusoidal pattern in general. Investigating a practical solution is an open problem of this research.

Reconstruction accuracy compared with the state-of-the-art [16] Our goal is to realize an interference-free surround structured lighting with a perspective projector, and is not to improve the the accuracy of the 3D shape reconstruction particularly. Compared with [16], their reconstruction resolution is limited not only by the projector/camera/mirrors calibration but also by the alignment and

the resolution of the Fresnel lens to realize the exact orthographic projection. On the other hand, our method does not have such additional factors, but has the aliasing issue above.

7. Conclusion

This paper proposed a new epipole-centered structured light pattern that realizes an interference-free surround lighting for mirror-based projector-camera systems. The key idea is to rectify the projector image based on the epipolar geometry between the real and the virtual projectors, and this achieved a code projection without collisions between the direct projection and the indirect projection via the mirror. Unlike the state-of-the-art [16] that employed an orthographic projector physically aligned in a specific configuration where the mirror normals are parallel to the projection direction, our method works with a regular perspective projector that is not necessarily aligned strictly.

The evaluation demonstrated that our pattern can significantly reduce code collisions in comparison with conventional horizontal patterns, and proved our interference-free projection concept in practice using real datasets.

As discussed in the last section, our method has several limitations. Our future study includes a pattern generation that can handle (1) multiple reflections to maximize the number of camera pixels contributing the 3D geometry measurement, and also (2) image aliasing problem based on the continuously-valued patterns and the phase-shifting technique [23, 28].

Acknowledgment The authors would like to thank anonymous reviewers for their insightful comments. This research is partially supported by JSPS Kakenhi Grant Number 26240023, 15J07706.

References

- [1] S. Agarwal, N. Snavely, I. Simon, S. M. Seitz, and R. Szeliski. Building rome in a day. In *Proc. of ICCV*, 2009. 1
- [2] B. Atcheson, I. Ihrke, W. Heidrich, A. Tevs, D. Bradley, M. Magnor, and H.-P. Seidel. Time-resolved 3d capture of non-stationary gas flows. In *SIGGRAPH Asia*, pages 132:1–132:9, 2008. 1
- [3] G. J. Brostow, C. Hernández, G. Vogiatzis, B. Stenger, and R. Cipolla. Video normals from colored lights. *IEEE TPAMI*, 33(10):2104–2114, October 2011. 8
- [4] C. Cagniard, E. Boyer, and S. Ilic. Free-form mesh tracking: A patch-based approach. In *Proc. of CVPR*, pages 1339–1346, 2010. 2
- [5] D. Cremers and K. Kolev. Multiview stereo and silhouette consistency via convex functionals over convex domains. *IEEE TPAMI*, pages 1161–1174, 2010. 1, 2

- [6] A. W. Fitzgibbon, G. Cross, and A. Zisserman. Automatic 3d model construction for turn-table sequences. In *Proceedings of SMILE Workshop on Structure from Multiple Images in Large Scale Environments*, pages 154–170, 1998. 2
- [7] K. Forbes, F. Nicolls, G. D. Jager, and A. Voigt. Shape-from-silhouette with two mirrors and an uncalibrated camera. In *Proc. of ECCV*, 2006. 2
- [8] Y. Furukawa and J. Ponce. Accurate, dense, and robust multi-view stereopsis. In *Proc. of CVPR*, pages 1–8, 2007. 1, 2
- [9] J. Gall, C. Stoll, E. D. Aguiar, C. Theobalt, B. Rosenhahn, and H. Peter Seidel. Motion capture using joint skeleton tracking and surface estimation. In *Proc. of CVPR*, 2009. 2
- [10] J. Gregson, M. Krimerman, M. B. Hullin, and W. Heidrich. Stochastic tomography and its applications in 3d imaging of mixing fluids. In *Proc. of ACM SIGGRAPH*, pages 52:1–52:10, 2012. 1
- [11] M. Havlena, A. Torii, and T. Pajdla. Efficient structure from motion by graph optimization. In *Proc. of ECCV*, pages 100–113, 2010. 1
- [12] C. Hernandez Esteban, G. Vogiatzis, and R. Cipolla. Multi-view photometric stereo. *IEEE TPAMI*, 30:548–554, 2008. 2
- [13] K. Ikeuchi, T. Oishi, J. Takamatsu, R. Sagawa, A. Nakazawa, R. Kurazume, K. Nishino, M. Kamakura, and Y. Okamoto. The great buddha project: Digitally archiving, restoring, and analyzing cultural heritage objects. *IJCV*, 75:189–208, 2007. 1, 2
- [14] K. H. Jang, D. H. Lee, and S. K. Jung. A moving planar mirror based approach for cultural reconstruction. *Computer Animation and Virtual Worlds*, 15(3-4):415–423, July 2004. 2
- [15] M. Kimura, M. Mochimaru, and T. Kanade. Projector calibration using arbitrary planes and calibrated camera. In *Proc. of CVPR*, pages 1–2, 2007. 2
- [16] D. Lanman, D. Crispell, and G. Taubin. Surround structured lightning: 3-d scanning with orthographic illumination. In *CVIU*, pages 1107–1117, November 2009. 1, 2, 3, 8
- [17] H. Li, E. Vouga, A. Gudym, L. Luo, J. T. Barron, and G. Gusev. 3d self-portraits. *Proc. of ACM SIGGRAPH Asia*, 32(6), November 2013. 2
- [18] D. Moreno and G. Taubin. Simple, accurate, and robust projector-camera calibration. In *Proc. of 3DIMPVT*, pages 464–471, 2012. 1, 2
- [19] N. Morris and K. N. Kutulakos. Dynamic refraction stereo. In *Proc. of ICCV*, pages 1573–1580, 2005. 1
- [20] M. Pollefeys, R. Koch, M. Vergauwen, and L. Van Gool. Hand-held acquisition of 3d models with a video camera. In *Proc. of 3DIM*, pages 14–23, 1999. 2, 3
- [21] R. Sagawa, K. Sakashita, N. Kasuya, H. Kawasaki, R. Furukawa, and Y. Yagi. Grid-based active stereo with single-colored wave pattern for dense one-shot 3d scan. In *Proc. of 3DIMPVT*, pages 363–370, 2012. 2
- [22] J. Salvi, J. Pages, and J. Batlle. Pattern codification strategies in structured light systems. *Pattern Recognition*, 37(4):827–849, April 2004. 1, 2
- [23] S. Savarese, J.-Y. Bouquet, and P. Perona. 3d depth recovery with grayscale structured lighting. Technical report, California Institute of Technology, 1999. 8
- [24] J. Starck, A. Hilton, and G. Müller. Volumetric stereo with silhouette and feature constraints. In *Proc. of BMVC*, pages 1189–1198, 2006. 1, 2
- [25] T. Tung, S. Nobuhara, and T. Matsuyama. Complete multi-view reconstruction of dynamic scenes from probabilistic fusion of narrow and wide baseline stereo. In *Proc. of ICCV*, pages 1709–1716, 2009. 1, 2
- [26] D. Vlasic, P. Peers, I. Baran, P. Debevec, J. Popović, S. Rusinkiewicz, and W. Matusik. Dynamic shape capture using multi-view photometric stereo. In *Proc. of ACM SIGGRAPH Asia*, pages 174:1–174:11, 2009. 2
- [27] G. Vogiatzis, C. Hernandez, P. Torr, and R. Cipolla. Multi-view stereo via volumetric graph-cuts and occlusion robust photo-consistency. *IEEE TPAMI*, 29(12):2241–2246, 2007. 1, 2
- [28] S. Yamazaki, M. Mochimaru, and T. Kanade. Simultaneous self-calibration of a projector and a camera using structured light. In *Computer Vision and Pattern Recognition Workshops*, pages 60–67, 2011. 1, 2, 8
- [29] Z. Zhang. A flexible new technique for camera calibration. *IEEE TPAMI*, 22(11):1330–1334, November 2000. 2